

# Calibration of Numerical Model Applied to a Shear Zone Located on a Slope in an Open Pit Mine—Case History

Evandro Moraes da Gama, Bruno C. R. da Silva

Department Mining Engineering, Federal University of Minas Gerais, Minas Gerais, Brazil  
Email: evandrodagama@gmail.com

Received October 14, 2011; revised November 28, 2011; accepted December 16, 2011

## ABSTRACT

The instability of a pit mine slope diagnostic caused by the slipping of a localized deep shear zone is described. The slope was designed on ultra basic, serpentine and metabasite rock formations with an angle varying from 40 to 45 degrees. The perturbed slope zone was classified as RMR 12 and the non-perturbed zone as RMR 75. The boundary of these zones is defined as the shear zone. The pit slope was field mapped in detail and the mechanical properties of the rock were obtained through a laboratory test. The lab data were further processed using the RMR mechanical classification system. The Distinct Elements Code numerical modeling and simulation software was used to design the pit slope. The model was calibrated through topographic mapping of the points on the ground. The task of calibrating a numerical model is far from simple. Exhaustive attempts to find points of reference are required. The mechanical behavior in function of the time factor is a problem that has yet to be solved. The instant deformation generated in the numerical model generated functions that can be compared with the deformations of quick shifts acquired in the topographic monitoring. SMR is indeed more often recommended for Pit Slopes, though the fact that we have used RMR does not invalidate the classification for the modeling effect. The main parameters such as spacing, filling, diving direction and continuity allow for compartmentalization of the modeled area. The objective of the modeling was not to project slopes because this massif was undergoing a progressive slow rupture. The objective of the modeling was to study the movement of the mass of rock and its progressive rupture caused by a shear zone.

**Keywords:** Calibrated Modeling; Shear Zone; Slope and Stability

## 1. Introduction

The term shear zone [SZ] generally refers to an area close to where parallel boundary shear deformations are located. The shear zones are formed by the relative movement of blocks of non-deformed, brittle rocks located on opposite sides moving in opposite directions. The shear zone moves on a parallel plane between the blocks as a result of the movement of the blocks towards both sides. This plane is called the shear plane. The shear zones can be divided into ductile shear, ductile-brittle and fragile zones [1].

Sama Mineração de Amianto has two serpentinite pits which appear to overlap metabasites with little schistosity. The main structures for the stability of slopes are foliations; brittle-ductile shear in fault zones. Ductile-brittle shear and fault zones appear in profusion in the open pit forming a cross network. The shear zones have variable extensions reaching up to several tens of meters. Many of them show evidence of having moved more than once.

Tailings vary on a scale of decimeters. They can be broadly classified into three groups. The first group com-

prises the areas of ductile shear formed under the mylonitic foliation for S1. These areas have a flat curve shape, in order to circumvent almond lentiform bodies of deformed serpentinites, **Figure 1**.

The second group consists of fragile and ductile zones and resembles a type of oblique fault inclined either to the right or to the left. Those groups are discordant from S1 and are related to the serpentinites with the most significant mineralization. The stability of slopes is constrained mainly by the ductile shear zones, which are divided into lenses, which separate the lenses of decametric

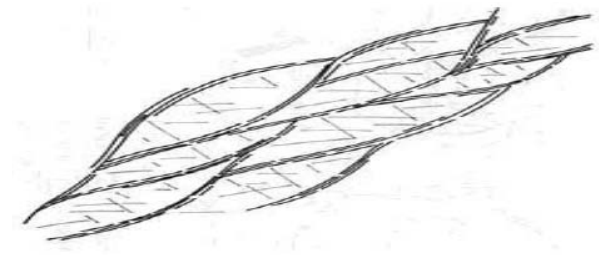


**Figure 1. Profile diagram showing the anastomosed shear zones isolating blocks in the form of almonds [2].**

thicknesses from less deformed rocks. This paper describes a diagnosis of the destabilization of a slope located on the eastern side of an open pit caused by the slow slide into depth of a shear zone, identified as a member of group 1.

This diagnosis was obtained through a detailed mapping of the slope and field instrumentation, considering the geomechanical properties based on geomechanical classification and, finally, a numerical model was produced using the Distinct Elements Code software [3].

The set of information (detailed mapping, monitoring, topographical and geomechanical properties obtained in laboratory tests and geomechanical classification applied to a numerical model) allowed for the development of a calibrated model of the eastern open pit slope. **Figure 2** shows a schematic of a calibrated model.

A calibrated model is a numerical geomechanical model that is a synthesis of the main geomechanical structures present endowed with geomechanical properties with this model being subjected to various forces. In our case the massif is subjected only to gravity as its structural mass is characterized by discontinuities to which were attributed geomechanical properties. This massif was monitored using topographical markers at studied and defined locations. When comparing the movement events measured using topography with the movement events calculated at pre-defined points, which were the same as those used in for the topographical markers, in the mathematical model, we are effectively calibrating the model. The comparisons between the movements obtained with the topographical instruments and those

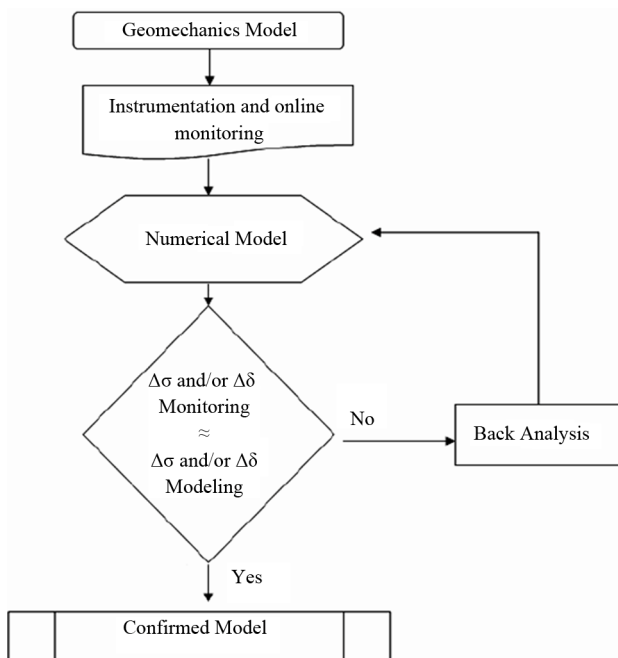


**Figure 2.** Schedule of calibrated explanatory model.

obtained from the model allow the mathematical model to be calibrated and thus more real and less theoretical. These comparisons are shown in the following pairs of **Figures: 10 & 11, 12 & 13, 14 & 15 and 16 & 17.**

## 2. Localized Structural Modeling

The stability of an open pit is determined by both the depths of the shear zone (SZ) and the face of the open pit slope. This parameter has to be balanced with the thickness, fill, shape (flat and/or anastomosed) and water level in the SZ and, especially, with the blasting plan implemented.

Two large fault arrays block open pits A and B. The open pit in this direction has failed in a NW-SE direction, dipping to the south. Between the two open pits there is a fault running in an E-W direction diving to the southern slope in the middle section of the fracture to the west, where the cohesion of the volumes of rock are reduced and separated by shear zones and traction fractures.

The mass is behaving like a set of blocks limited in depth by shear zones. Traction fractures are found together with the SZs. The movement of the blocks in the opening SZs causes traction fractures that are almost perpendicular to the SZs. **Figure 3** below illustrates the movement of the kinematical disruption of the eastern slope [4].

This shear zone was mapped in detail with the aid of a drilling campaign and detailed description of the borehole. The model set is shown below.

The descriptions showed that the SZ is:

Borehole 01 - 80 meters deep where a crack was found filled with clay.

Borehole 02 - 34 meters deep where there were heavily fractured serpentinites.

Borehole 03 - 21 meters deep where there is a transition from a highly fractured serpentinite to a slightly fractured serpentinite zone with a gap.

Borehole 04 - 50 meters deep where there is an extremely fractured passage of serpentinites to slightly fractured serpentinites.

The destabilization involves the movement of a 164, 824 m<sup>3</sup> mass of rock. The photos below show the location.

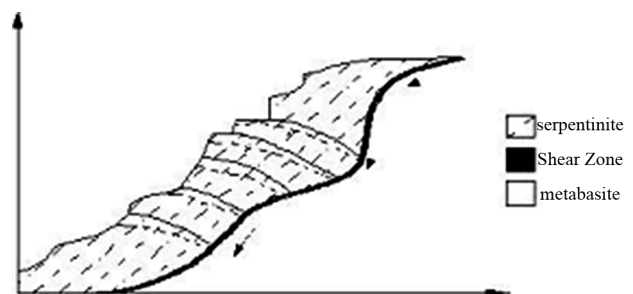


**Figure 3.** Kinematical disruption.

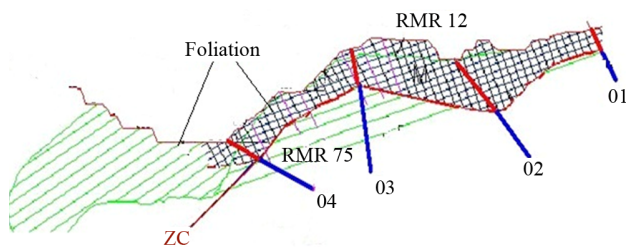


**Figure 4.** SZ Shear Zone, boreholes 01, 02, 03, and 04 RMR = 12 rock mass fractured, RMR = 75 rock mass no fracture.



**Figure 5.** Slope top disjuncted.

Through a detailed description of the fractures with the aid of detailed topography and measurements taken with a compass, it was possible for us to build a topography model, adding the mapped fractures.

### 3. Laboratory Test

There are two geometric areas. The first one is above the sliding surface (SZ) with spacing between blocks ranging from 7.0 m to 5.0 m from south to north in an east-west direction. This is the area which was directly affected by the landslide. The second one is below the sliding surface (SZ) with spacing between blocks of about 10.0 m to 7.0 m from south to north in an east-west direction.

Laboratory tests were conducted by IPT Brazil [5], a benchmark in South America for geomechanical properties of rocks and Cojean [6] focused on the shear strength, uniaxial compressive strength using the indirect tensile strength method. Because the samples did not have the proper structure to undergo direct tensile strength tests, a diametral compression or indirect tensile strength, was applied, as suggested by ISRM—the International Society of Rock Mechanics.

The north-south (305/86 SW family—foliation) 66/30 and NW (family of discontinuity) discontinuity rigidity properties were calculated using the RMR methodology for the boreholes

The RMR used for the area before the SZ was 12 and,

for the area after the SZ, it was 75. The calculation of the discontinuity rigidity properties was based on [7].

The UCS of 93.90 MPa refers to the rocky matrix of the serpentinite with no discontinuities and the cohesion equal to zero is due to the foliation which is an open discontinuity and therefore presents a cohesion of zero with its resistance attributed to the friction angle of 22.10 degrees and Kn stiffness of 249.19 MPa and Kt 95.18 MPa. The foliation and the 66°/30° family NW inside SZ are within the shear zone and therefore are working with a cohesion of zero or very near zero. This shows that the movement is greater through these discontinuities.

### 4. Calibrated Numerical Model

The numerical model was calibrated using four points following exhaustive research to identify which points have displacements similar to the four points which were topographically monitored. Metal rods introduced into 2-inch holes and equipped with electronic sticks and monitored with total station. Four topographical points were monitored for 672 days. The numerical model and monitored points are shown in **Figure 7** below. The topographic monitoring shown by **Figures 6, 8, 10** and **12**, is referenced to topographical coordinates on the y axis and the x-axis refers to time in hours. The comparisons of displacements commented on below show vertical displacement in metric units. These displacements are variations between the metric topographic coordinates.

The graphs below, **Figures 10 & 11, 12 & 13, 14 & 15** and **16 & 17**, show and compare the results gathered at the monitoring points of topographic displacement and their respective calibrated modeling points 55, 22, 30 and 25 in **Figure 9**.

**Figure 10** shows the monitoring of topographic point 4 and **Figure 11** shows point 30 of the calibrated numerical model. There is a rapid vertical displacement, suggesting the accommodation of the blocks at the most fractured



**Figure 6.** Ramp access destroyed.



Figure 7. Front View of the Break.

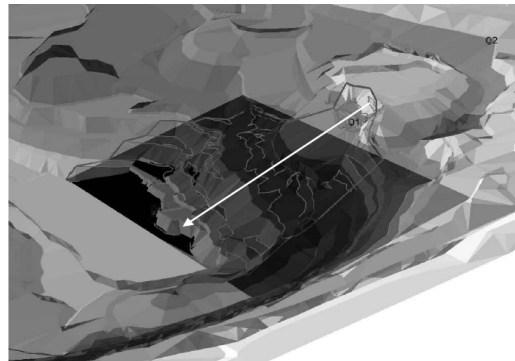


Figure 8. Topography model with structural fractures, boreholes 01, 02, 03 and 04, white arrow aligned with topographical monitoring.

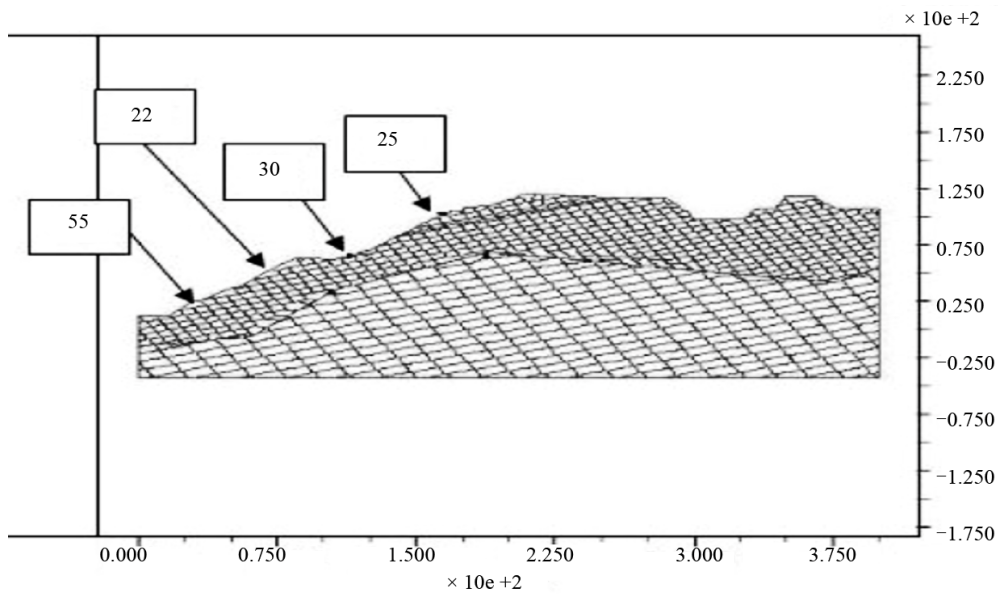


Figure 9. Numerical model and monitoring points.

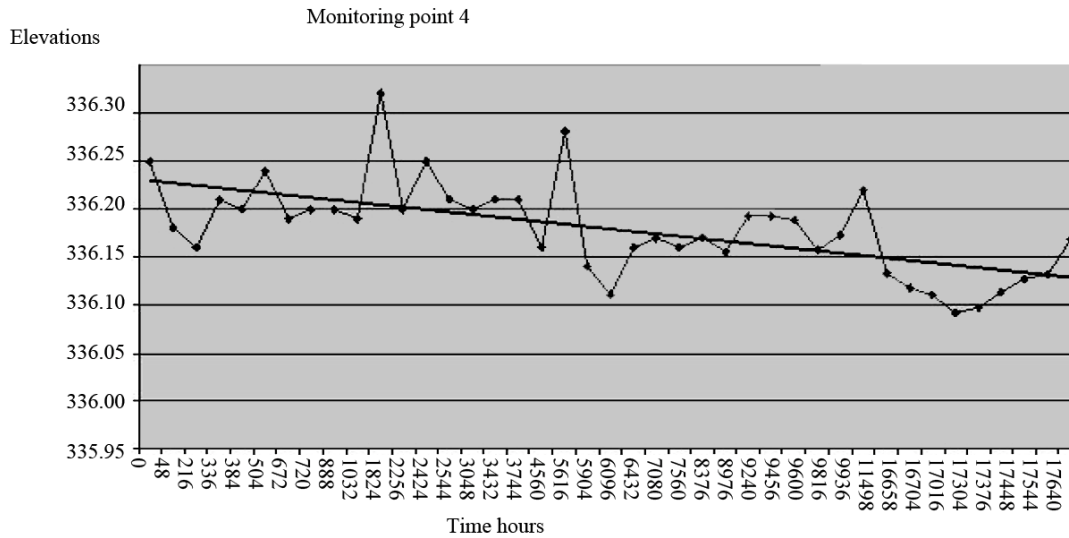


Figure 10. Point 4 topography monitoring.

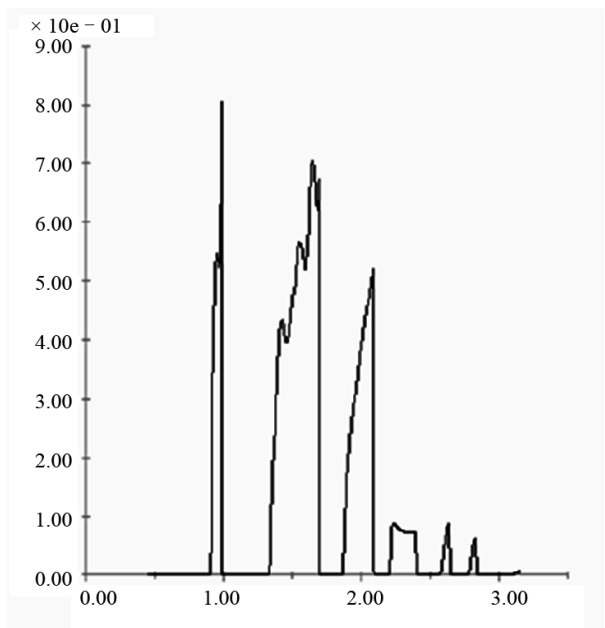


Figure 11. Point 30 calibrated modeling.

zone of the ramp, which were the largest blocks. The order of magnitude of the vertical displacements ranged from 0.13 to 0.32 m.

We observed the same trend in the accommodation blocks with a vertical variation of between 0.1 and 0.8 m. The numerical model was not able to show a temporal variation as the topographic monitoring was. We did notice, however, that the extent to which the 0 to 3 UDEC cycles are applied determines the vertical displacement decrease.

Figure 12 shows the monitoring of the topographic point and Figure 13 shows point 25 of the calibrated numerical model. Section 1, which is monitored via topo-

graphy, shows a maximum displacement of 1.40 m between 0 and 5616 hours. At two peaks, displacements at 1834 hours and 5616 hours were observed. The displacements and absolute magnitude are located between 0.30 and 0.80 m. These shifts are associated with accommodation blocks. After 16,704 hours, shifts are on the order of 0.25 m with a tendency to remain constant for some time.

The point 25 of the calibrated model shows two points of maximum displacement of 0.30 m and 0.15 m. After being stabilized at 0.25 m, we kept it this way until the blocks had been stabilized.

Figure 14 shows the topographic monitoring of section 2 and Figure 15 shows the corresponding point in the numerical model.

Between 0 and 1032 hours there is a maximum displacement of 1.1 m. At the 1032nd hour we have a peak displacement of 1 meter. After this peak, shifts tend to stay at a constant topographic level (325), and show a second set of displacements at elevation 324.5. Figure 11 shows point 35 of the calibrated model where we have the same trend.

There is a rapid increase in deformation to 0.18 m. Then we have variations of displacement close to 0.18 m. Finally, the model stabilizes at 0.175 m. This point does not show an order of magnitude for displacement similar to the topography and neither do monitoring points 25 and 30. Figure 14 corresponds to the third point of topographical tracking and Figure 15 shows the corresponding point in the calibrated model.

Figure 16 shows a progressive shift from 1 to 2 meters over a 426-hour interval, stabilizing at topographic elevation 332.

From this point we have a gradual stabilization, possibly temporary, with a maximum displacement of 0.5 m.

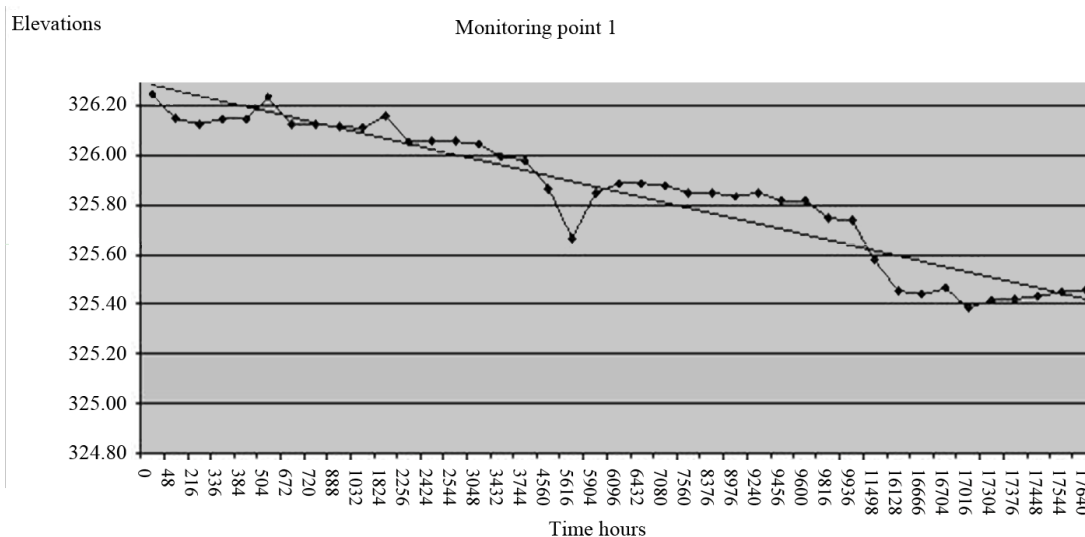


Figure 12. Point 1 topography monitoring.

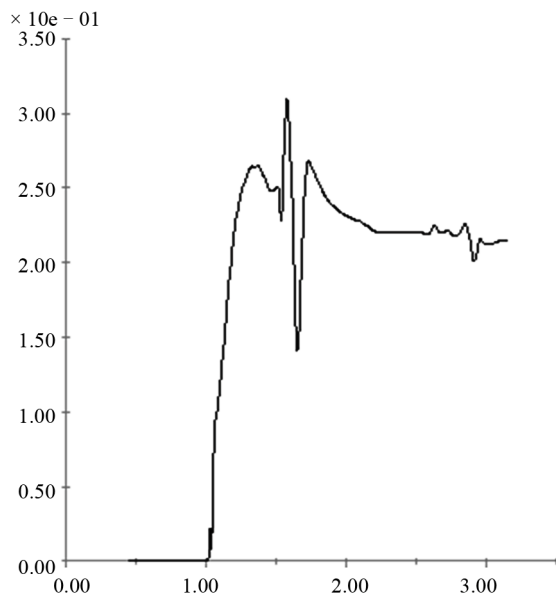


Figure 13. Point 25 calibrated modeling.

Figure 17 corresponds to the numerical model and shows the same trend. There is a quick shift to 0.09 m after a gradual stabilization near 0.085 m. But this point does not show an order of magnitude for displacements similar to the displacements obtained through the topographic monitoring.

### 5. Discussion

The curves for the displacements obtained through the monitoring show topographic features very similar to the displacement curves obtained in the numerical model.

Paragraphs 30 and 25 of the numerical model show an order of magnitude for the displacements that is compatible with the numerical model. However, points 55 and 22 do not present an order of magnitude for the displacements that is compatible with the topographic monitoring.

The topographically monitored points are spaced 100 meters apart. The blocks are disconnected, and their friction coefficient is the only stabilizing factor. The more density there is the greater are the friction and the safety. Thus, the orders of magnitude for the displacements of points 55 and 22, which were similar to those topographic monitoring points, should have been on blocks that were separated or not engaged in the model. But it is not an easy task to consider all the blocks and choose those with mechanical behavior compatible with the real magnitudes of the displacements, obtained from topographic monitoring.

However the interpretation of physical and mechanical stability is maintained because the curves show displacement functions very similar and comparable to those obtained in the topographic monitoring.

The movements are typical of disconnected blocks where small deformations accumulate over long periods and suffer large deformations faster than usual. The fastest movements were caused by the dismantling with explosives of the front slope in the studied area.

It was observed that the size of the displacement of Figures 6-8 ranges from 0.15 to 0.30 m. Point 4 is in the highest elevation of the ramp followed by monitoring points 1, 2 and 3. There is a clear trend towards an increase in the vertical displacement over time.

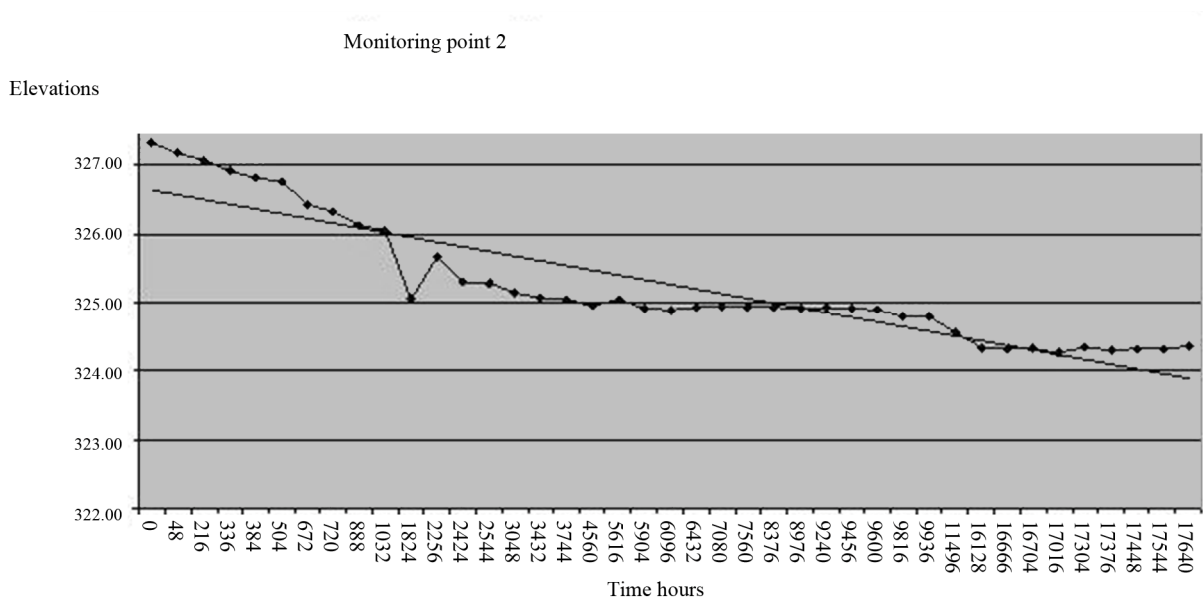


Figure 14. Point 2 topography monitoring.

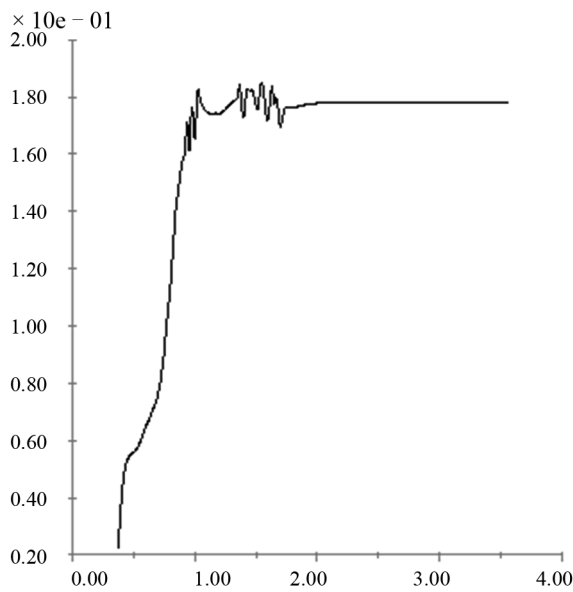


Figure 15. Point 55 calibrated modeling.

The Topography monitoring used did not allow for a continuous evaluation of the data with shorter time intervals. On the other hand, kn (Normal Joint stiffness) and kt (Joint shear stiffness) applied to the model, can impose minor displacements between the blocks. All these factors make the numerical calibration of the model more difficult [4].

The numerical modeling was performed using the

UDEC: Universal Distinct Element Code software, version 3.0 Itasca Consulting [8].

**5.1. Input Data and Assumptions in the Model**

The model was based on the size of the blocks in Figure 4. The results of the field mapping were used for the biggest blocks which have dimensions (in meters) of  $6.20 \times 4.50 \times 5.20 \times 2.30$  and  $4.60 \times 2.80$ . The input parameters for a numeric geomechanical model are the mechanical properties shown in Table 1 and the discontinuities mapped in the field. As a synthesis of a structural model, the model presented may appear simple. However, the complexity of this model lies in the fact that there is a numerical convergence of the results.

**5.2. Results**

In Figure 18 the dark lines show the model simulation of the slip surfaces of slope, which are within the friction limits, or that is those that are collapsing. They indicate that the SZ, represented by the thick, dark line is found in the process of collapsing. The same occurs at several points of the 66/30 NW foliation family, which are also in process of free shear.

Figure 19 shows that, through the simulation model, maximum displacements of  $4.41 \times 10^{-2}$  m were found, which are represented by the regions highlighted by the thick, dark lines. At such discontinuity points, the displacement opens and continues moving.

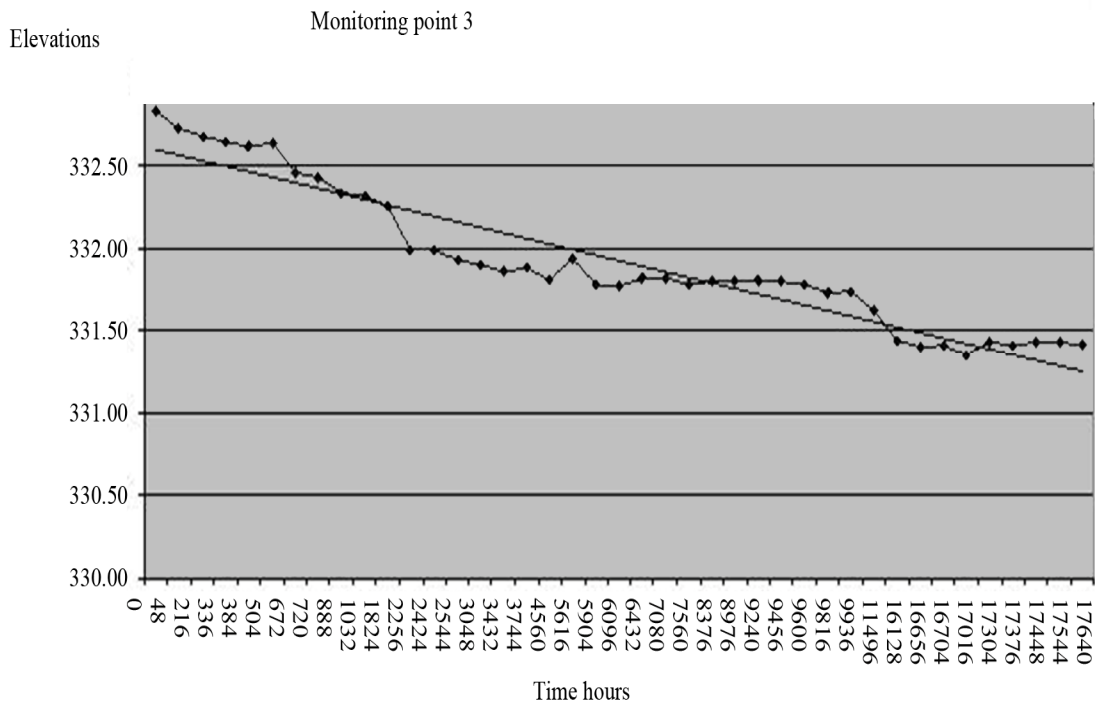
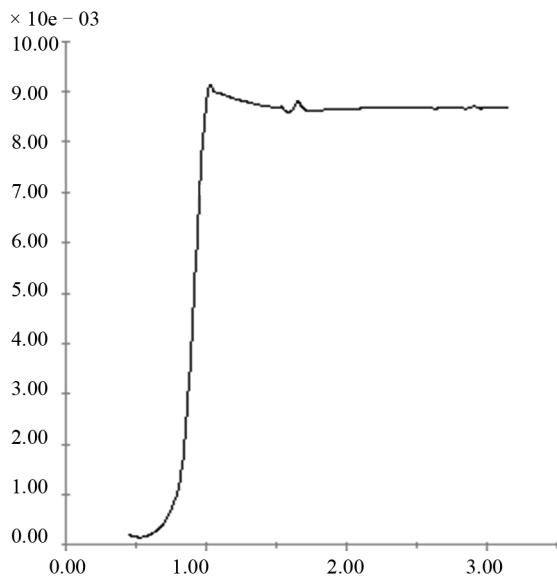


Figure 16. Point 3 topography monitoring.

**Table 1. Results of mechanical laboratory tests.**

<i>Lythotypes</i>	C Mpa	$\Phi$ grade	$\sigma_c$ Mpa	$\sigma_t$ Mpa	$\gamma$ t/m <sup>3</sup>	G Mpa	K Mpa	Kn Mpa	Kt Mpa
Serpentinite Matrix	1.10	44.90	93.90	11.07	2.63	17521.00	37963.00		
Foliation inside SZ	0.00	22.10						249.18	95.81
66°/30° Family NW inside SZ	0.09	29.60						249.18	95.81
Foliation after SZ	0.26	26.90						4047.82	1553.60
66°/30° Family NW after SZ	0.97	58.50						4047.82	1553.60

C: cohesion,  $\theta$ : friction angle,  $\sigma_c$ : Uniaxial Compression,  $\sigma_t$ : Indirect Tension,  $\gamma$ : density, G: Shear modulus, kn: Normal Joint stiffness, kt: Joint shear stiffness.



**Figure 17. Point 22 calibrated modeling.**

### 6. Conclusions

The destabilization of a shear zone, shown in this paper, is a slow and continuous process.

Topographic monitoring, especially from point 04 when compared to the 30th point shows a weak relationship with the displacement of the surface of the tracked slope and a small similarity to the numerical model developed.

Factors contributing to this destabilization are closely linked to the angles of the slope used in the plowing operations and placement of embankments with a geometric relationship to the fault and SZ located near the face of the dismantled slope.

This analysis shows the need for a detailed map of the structural stability of the open pit in operation.

The task of calibrating a numerical model is far from simple. Exhaustive attempts to find points of reference are required. The time factor is a problem that has yet to be solved, but, for now, the deformation generated in the

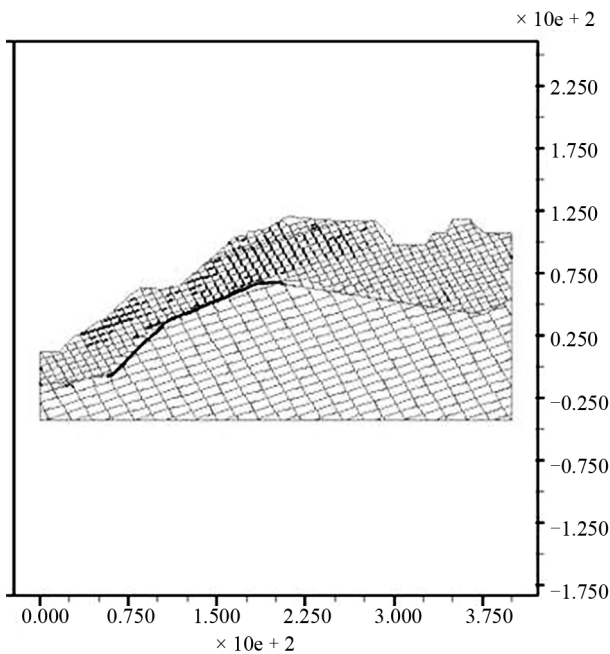


**Figure 18. Joint now at shear limit shown in darker lines.**

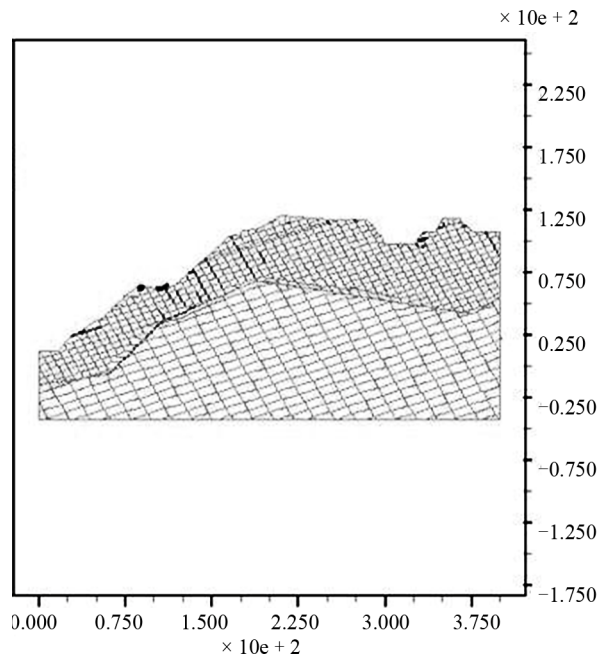


**Figure 19. Shear displacement shown in darker lines.**

numerical model generated functions that can be compared with the deformations with quick shifts acquired through topographic monitoring.

The topography does not allow for the tracking of a continuous data record. With a continuous record of, for example, one measurement per minute, perhaps we'd have a better calibration of the model [9].

### REFERENCES

- [1] J. G. Ramsay, "Shear Zone Geometry a Review," *Journal of Structural Geology*, Vol. 2, No. 1-2, 1980, pp. 83-89. [doi:10.1016/0191-8141\(80\)90038-3](https://doi.org/10.1016/0191-8141(80)90038-3)
- [2] Y. Hasuo, F. S. Magalhaes and A. F. Mangolin, "Applied Structural Geology," 1992, pp. 363-382.
- [3] P. A. Cundall, "Numerical Modeling of Jointed and Faulted Rock in Mechanics of Jointed and Faulted Rock," A. A. Balkema, Rotterdam, 1990, pp 11-18.
- [4] E. Gama and L. Borrher, "Efeito de uma zona de cisalhamento na estabilidade de um talude de mineração". In: IV Congresso Brasileiro de mina á ceu aberto e mina subterranea, Belo Horizonte. MG Brasil, 2006.
- [5] IPT, "Relatório de Ensaios," Instituto de Pesquisas Tecnológicas, Sama Mineração, 1996.
- [6] R. Cojean and S. Curtil, "Rapport d'Avancement des travaux de Thése," ARMINES Centre de Geologie de L'Ingenieur, Paris, 1995.
- [7] P. A. Cundall and R. D. Hart. "Development of Generalized 2-D and 3-D Distinct Element Modeling Programs for Jointed Rock," Itasca Consulting Group, US Army Corps of Engineers, Itasca Consulting Group, 1985.
- [8] D. Billaux, F. Dedecker and P. Cundall, "A Novel Approach to Studying Rock Damage: The Three Dimensional Adaptive Continuum/Discontinuum Code," *Proceedings of EUROCK 2004 & 53rd Geomechanics Colloquium*, Ed. Schubert, 2004, pp. 723-728.
- [9] E. M. Gama. "Rock Mechanics Applied to Mining," EEUFMG, Vol. 1, 2005.